Journal of Geophysical Research: Oceans

RESEARCH ARTICLE
10.1029/2018JC014320

Interconnectivity Between Volume Transports Through Arctic Straits

Agatha M. de Boer[1], Estanislao Gavilan Pascual-Ahuir[2], David P. Stevens[3], Léon Chafik[4], David K. Hutchinson[1], Qiong Zhang[5], Louise C. Sime[6], and Andrew J. Willmott[7]

[1]Department of Geological Sciences and Bolin Centre for Climate Research, Stockholm University, Stockholm, Sweden, [2]School of Natural and Environmental Sciences, Newcastle University, Newcastle upon Tyne, UK, [3]Centre for Ocean and Atmospheric Sciences, School of Mathematics, University of East Anglia, Norwich, UK, [4]Department of Meteorology and Bolin Centre for Climate Research, Stockholm University, Stockholm, Sweden, [5]Department of Physical Geography and Bolin Centre for Climate Research, Stockholm University, Stockholm, Sweden, [6]British Antarctic Survey, Cambridge, UK, [7]School of Mathematics, Statistics and Physics, Newcastle University, Newcastle upon Tyne, UK

Key Points:
- Interannual volume transport variability in Arctic straits must be interconnected to maintain Arctic Ocean mass balance
- Transports through both the Bering Strait and Canadian Archipelago are correlated to Nordic Seas transport and not to each other
- Bering Strait transport perturbations are preferentially adjusted in the Nordic Seas due to shelf and strait geometry

Correspondence to:
A. M. de Boer,
agatha.deboer@geo.su.se

Citation:
de Boer, A. M., Gavilan Pascual-Ahuir, E., Stevens, D. P., Chafik, L., Hutchinson, D. K., Zhang, Q., et al. (2018). Interconnectivity between volume transports through Arctic straits. *Journal of Geophysical Research: Oceans*, *123*. https://doi.org/10.1029/2018JC014320

Received 28 JUN 2018
Accepted 6 NOV 2018
Accepted article online 9 NOV 2018

Abstract Arctic heat and freshwater budgets are highly sensitive to volume transports through the Arctic-Subarctic straits. Here we study the interconnectivity of volume transports through Arctic straits in three models; two coupled global climate models, one with a third-degree horizontal ocean resolution (High Resolution Global Environmental Model version 1.1 [HiGEM1.1]) and one with a twelfth-degree horizontal ocean resolution (Hadley Centre Global Environment Model 3 [HadGEM3]), and one ocean-only model with an idealized polar basin (tenth-degree horizontal resolution). The two global climate models indicate that there is a strong anticorrelation between the Bering Strait throughflow and the transport through the Nordic Seas, a second strong anticorrelation between the transport through the Canadian Arctic Archipelago and the Nordic Seas transport, and a third strong anticorrelation is found between the Fram Strait and the Barents Sea throughflows. We find that part of the strait correlations is due to the strait transports being coincidentally driven by large-scale atmospheric forcing patterns. However, there is also a role for fast wave adjustments of some straits flows to perturbations in other straits since atmospheric forcing of individual strait flows alone cannot lead to near mass balance fortuitously every year. Idealized experiments with an ocean model (Nucleus for European Modelling of the Ocean version 3.6) that investigate such causal strait relations suggest that perturbations in the Bering Strait are compensated preferentially in the Fram Strait due to the narrowness of the western Arctic shelf and the deeper depth of the Fram Strait.

Plain Language Summary The Arctic is one of the most fragile places on the Earth, facing double the rate of warming as the rest of the globe. This warming is partly due to melting of sea ice because open water reflects less sunlight than ice. One of the major controls on Arctic sea ice concentration is the heat flowing into the Arctic through its straits. However, due to the harsh conditions in the Arctic, there are limited long-term observations of the currents flowing through these straits. Here we turn to climate models to investigate these Arctic straits flows and in particular focus on how flows into and out of the Arctic balance each other. We find that in some instances specific pairs of strait flows are simultaneously affected by large-scale atmospheric. In other instances, the inflow through one strait flows out through another distant strait because of the way the ocean floor guides the currents. Traditionally, the flows through Arctic straits are studied in relation to local forces such as wind and sea level. Our work suggests value in a more holistic approach; one that also accounts for flow changes in a strait as a response to flow changes in other straits.

1. Introduction

The Arctic climate system is experiencing a rapid rate of change, which is expected to continue over the next few decades (Intergovernmental Panel on Climate Change, 2013). Many elements of this system are sensitive to the freshwater and heat exchange through the straits connecting the Arctic and Subarctic ocean basins. Freshwater exchange through the Arctic straits affects the stratification in the Arctic and the North Atlantic and the strength of the Atlantic Meridional Overturning Circulation (AMOC; Hu et al., 2010; Hu & Meehl, 2005; Mauritzen & Häkkinen, 1997; Otterå et al., 2003; Sevellec et al., 2017; Yang et al., 2016), while the response of the AMOC to freshwater forcing is particularly sensitive to the route that freshwater takes from the Arctic to the Atlantic (Koenigk et al., 2007). Similarly, the rapidly declining sea ice cover, which has a strong positive feedback to Arctic warming, is sensitive to heat transport through the Arctic straits (Bhatt

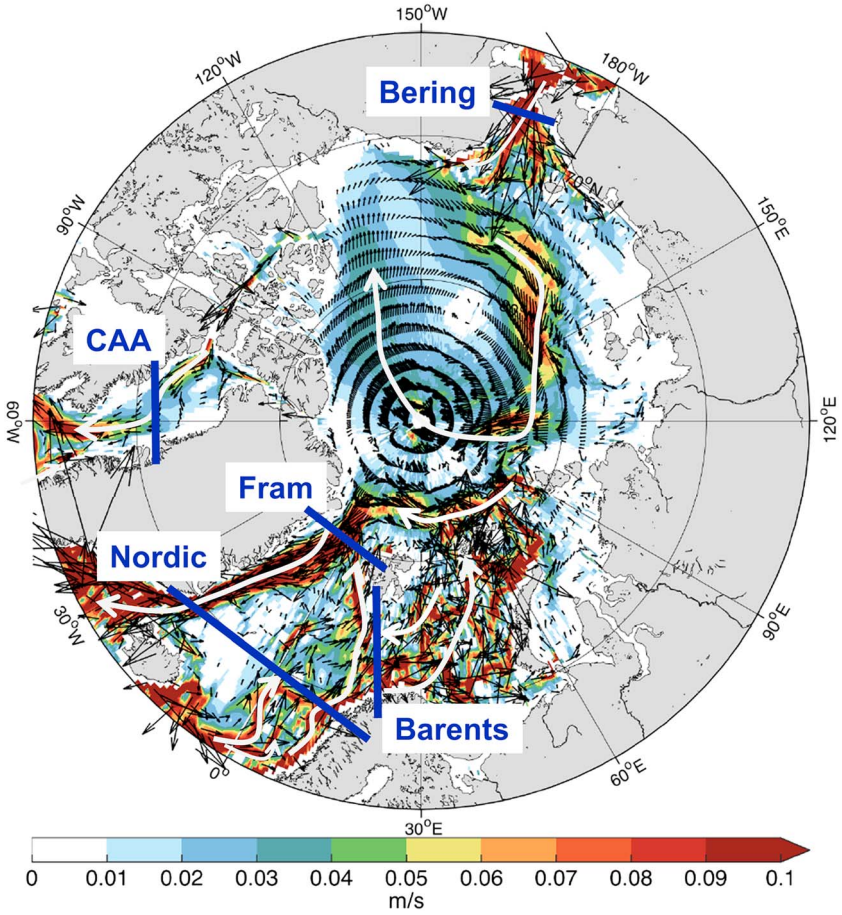

Figure 1. Surface current speed in High Resolution Global Environmental Model version 1.1 (HiGEM1.1), depth-averaged over the top 50 m and time-averaged over the last 20 years of the simulation. The direction of the currents is indicated by the black arrows, and the general sense of the circulation is also indicated by the white thicker arrows. Note that the circulation in the Barents Sea has a fine-scale pattern, which is not captured accurately in the simplified schematic. The blue sections indicate the Arctic straits considered in this study. (The sections follow latitude and longitude lines but are drawn straight here for convenience.)

et al., 2014; Stroeve et al., 2007). For instance, Woodgate et al. (2006) found that the increased heat input from the Pacific to the Arctic between 2001 and 2004 could melt 640,000 km^2 of thick sea ice.

The volume transports through the various Arctic straits have been measured and modeled for decades, and great progress has been made in understanding their driving mechanisms (Beszczynska-Möller et al., 2011; Dickson et al., 2000; Ingvaldsen et al., 2004; Lique & Johnson, 2015; Woodgate et al., 2015). However, connectivity between strait transports in the Arctic on annual and longer time scales remains poorly understood. Since the Arctic is a closed basin, a small volume flux imbalance on annual time scales would lead to large unrealistic sea level variations; for example, an anomaly of 0.1 Sv (1 Sv = 10^6 m^3/s) would lead to about 30 cm of mean sea level rise in the Arctic in one year (assuming an area of 10×10^6 km^2, which represents the area poleward of the sections for the Bering Strait, Canadian Arctic Archipelago (CAA), Fram Strait, and Barents Sea as indicated in Figure 1). This would be an order of magnitude larger than observed interdecadal sea level variability, which is a couple of centimeters, and also large compared to seasonal variability of about 9 cm (Armitage et al., 2016). The variability of the various Arctic Strait flows must therefore be coupled, which implies that not all strait volume transports can be attributed to local forcing all the time.

A variety of studies have looked at the connection between the transports through pairs of straits such as the CAA and the Nordic Seas (Lique et al., 2009) and the Fram Strait and Barents Sea opening (Lien et al., 2013). The flow into and out of the Arctic has also been studied in two separate applications of Godfrey's Island Rule. In the first application, the volume transport was calculated around the *island* of the Americas; thus,

calculating the transport from the Pacific to the Atlantic (De Boer & Nof, 2004a, 2004b) and in the second application, the circulation was determined around the island of Greenland (Joyce & Proshutinsky, 2007). In each case, the straits (or combination of straits) that transport the water in and out of the Arctic are predetermined and are equal and opposite by construct. Therefore, the Island Rule method sheds light on the dependence of the throughflow on wind and friction but not on the specific relationship between the variability in different Arctic straits.

In this study we wish to specifically address how strait flows relate to each other. In particular, we examine the interstrait connections that are a consequence of near-mass conservation in the Arctic on annual times scales. At present, this can only be studied in models because (a) the available transport observations though the Arctic straits are not in mass balance, even to first order and (b) the instrumented sections overlap for only five years (see section 3.1 for details on available observations). Here two global coupled climate models and an idealized polar basin ocean model are used to investigate the interannual variability of the Arctic straits volume transport. The two global climate models are the High Resolution Global Environmental Model version 1.1 (HiGEM1.1) model with a 1/3° horizontal ocean resolution and the Hadley Centre Global. Environment Model 3 (HadGEM3) model with a 1/12° horizontal ocean resolution. The HiGEM1.1 model has a 130-year control run and has been used extensively before (De Boer et al., 2013; Graham et al., 2012; Johnson et al., 2018; Roberts et al., 2009; Thomas, 2012), while the HadGEM3 model is a newer state-of-the-art model for which the control run is 39 years long (Williams et al., 2017). In both models, we calculate the correlations of the strait transports to each other and to five climate indices and find that the Bering Strait and the Canadian Arctic Archipelago throughflows are correlated to the volume transport through the Nordic Seas and not to each other. In the longer simulation of the HiGEM model, the sea level pressure, sea surface height (SSH), and wind stress are regressed against the transport time series in the main straits to investigate whether forcing mechanisms for respective strait flows are independent or whether there are large-scale forcing patterns that may force different strait transports simultaneously (see section 4.1). To investigate the causal correlation between strait flows that is the direct result of the adjustment of one strait to the transport anomaly in another (through for instance wave adjustments), we perform idealized circular-basin experiments in the NEMO3.6 ocean model (see section 4.2). It is beyond the scope of this work to fully explore this causal nature of the correlations, and in this study we focus on the response in the Arctic straits to a perturbation in the Bering Strait. In particular, we investigate what are the essential bathymetric characteristics of the Arctic Ocean basin that are required to capture the correlation between the Bering Strait and the Nordic Seas transports.

2. Models and Methods

2.1. HiGEM1.1

To study the interstrait relationships between Arctic strait volume transports as well as their relation to selected climate variables, we use the fully coupled climate model HiGEM1.1 (Roberts et al., 2009; Shaffrey et al., 2009). This model was developed by the UK High-Resolution Modelling Project and the UK-Japan Climate Collaboration. The horizontal resolution in the atmosphere is 5/6° latitude × 5/4° longitude with 38 levels in the vertical reaching from the surface to 39 km. The horizontal resolution in the ocean and sea ice components is 1/3° in both directions. The 5-500-m deep ocean comprises 40 unevenly spaced vertical layers varying from about 10 m thick at the surface to 300 m thick in the deep ocean. The ocean component is formulated on a spherical latitude-longitude grid, which has a singularity at the North Pole that is treated as a land point. Momentum dissipation occurs through a scale-selective biharmonic scheme. Lateral mixing of tracers uses the isopycnal formulation of Griffies (1998) with constant isopycnal diffusivity. The Gent and McWilliams (1990) adiabatic mixing scheme with a latitudinally varying thickness diffusion and the adiabatic biharmonic scheme of Roberts and Marshall (1998) are used to parameterize eddies and reduce noise in tracer fields, particularly at high latitudes. The atmospheric initial conditions are from the European Centre for Medium-Range Weather Forecasts (ECMWF) analyses, and the ocean initial conditions are from the 2001 World Ocean Atlas (Conkright et al., 2002). In this study, we make use of a 150-year simulation in which greenhouse gas concentrations have been kept constant at 1985 values (e.g., the CO_2 concentration is 345 ppm). The first 20 years were part of the model spin up and we use the last 130 years of model output for our analysis. It is a short spin up time but should be sufficient for this study because the ocean started from realistic

initial conditions and this study is primarily concerned with upper ocean currents and short-term variability thereof. All data are annually averaged and detrended for analysis.

2.2. HadGEM3

The strait correlations are also examined in a high-resolution version of the coupled model HadGEM3 GC3.1 (Williams et al., 2017). The model was developed by the Met Office as the basis of the United Kingdom's submission to the Coupled Model Intercomparison Project 6 (CMIP6). The horizontal resolution of the atmosphere is 25 km with 85 levels in the vertical reaching from the surface to 85 km. The ocean model is based on version 3.6 of the NEMO ocean model code (Madec, 2016). The horizontal resolution in the ocean and sea ice components is nominally 1/12° based on ORCA12 global tripolar grid of the NEMO framework (Madec, 2016). This grid has poles in land points in Antarctica, Siberia, and Canada and a reduction in the meridional grid spacing with increasing latitude to match the reduction in the zonal grid spacing. The ORCA12 grid thus provides a resolution of 9 km at the equator and 2 km in the Canadian Archipelago. The ocean comprises 75 unevenly spaced vertical levels varying from about 1 m thick at the surface to around 200 m thick at 5000 m. Further details of the ocean model can be found in Storkey et al. (2018). The model is computationally very expensive, which limits the length of simulations. In this study, we make use of a 39-year simulation performed under the ACSIS program (Sutton et al., 2017), in which greenhouse gas concentrations have been kept constant at 1950s values. The 28th year of the simulation was removed due to some missing output. All data are annual-averaged and the trends removed.

2.3. NEMO

In order to understand the causal relationship between strait transport variability, we conduct a series of process studies using the ocean model NEMO3.6 (Madec, 2016). The model domain is a circular step-shelf basin with three gaps, which represent the Nordic Seas, the Bering Strait, and the CAA. This initial study focuses on the adjustment of the circulation and strait transports to a perturbation in the Bering Strait. We are interested to see whether it leads preferentially to an adjustment in the Nordic Seas transport or in the CAA transport and how this may be affected by the bathymetry. The horizontal resolution of the model is $1/10° \times 1/10°$ with eight vertical levels with a constant thickness of 125 m, and the North Pole is located in the center of the grid. The periphery of the basin is set at 70°N, and the strait gap widths correspond roughly to the real strait dimensions at the latitude; that is, the Bering Strait width is 621 km, the CAA width is 652 km, the Barents Sea inflow width (in Nordic Seas) is 1,031 km, and Fram Strait outflow width (in Nordic Seas) is 637 km. The barotropic deformation radius here is 361 km. Laplacian eddy diffusion with a diffusivity of 500 m^2/s and linear bottom friction with a drag coefficient of 10^{-3} m/s are included in the momentum equations. The model is run in a barotropic mode. Following Luneva et al. (2012), a filtered nonlinear free surface algorithm is used, which is stable with relatively large time steps but damps the fast gravity waves and inertia-gravity waves. However, planetary waves and inertia-gravity waves with periods longer than 40 min are resolved using this time stepping method. (We performed a short simulation of 5 months without the filtering for one of the simulations, and the results were qualitatively similar.)

Three experiments are performed in different basin geometries (see section 4.2 for details). In each case, a control simulation is set up in which the strait volume transports are initially prescribed to correspond to the HiGEM1.1 model output (see Table 1). Thus, there is a Bering Strait inflow of 1.2 Sv, a CAA outflow of 0.8 Sv, an inflow of 3.6 Sv across the eastern half of the Nordic Seas strait (representing the Barents Sea inflow), and an outflow of 4 Sv across the western half of this strait (representing the Fram Strait outflow). As the model integration proceeds, the Bering Strait transport remains fixed, while the transports through the CAA and Nordic straits are modified using the Flather (1994) open boundary condition. In essence, this open boundary condition allows the difference between the prescribed and model transports to propagate out of the domain at the speed of external gravity waves. The boundary condition therefore deals with the initial discontinuity in the Nordic Seas gap by adjusting the inflow and outflow to the interior. The control simulations reach a steady state in 10 model years. Subsequently, the inflow through the Bering Strait is ramped-up from 1.2 to 2 Sv over a period of 1 year and the circulation during the transient adjustment to the new steady-state and the response in the CAA and Nordic Seas are studied.

Table 1
Mean Volume Transport and SD (in Sv) for the Five Strait Openings in HiGEM1.1 and HadGEM3, as Well as Estimates From Observations

	Bering	Nordic	CAA	Fram	Barents	Sum
Observations	1.0 ± 0.1		−1.7 ± 0.3	−2.2 ± 2.1	2.1 ± 0.4	−0.8
HiGEM1.1	1.2 ± 0.2	−0.6 ± 0.2	−0.8 ± 0.1	−4.0 ± 0.5	3.4 ± 0.5	−0.2
HadGEM3	1.1 ± 0.2	0.6 ± 0.4	−2.0 ± 0.4	−2.3 ± 0.5	3.0 ± 0.4	−0.2

Note. See text for sources.

2.4. Calculation of Correlations

The three main straits or openings connecting the Arctic and Subarctic oceans are the Bering Strait, the CAA, and the Nordic Seas opening. The transport through the Nordic Seas enters the Arctic either through the Fram Strait or the Barents Sea. The flows through these latter two branches are considered individually because they behave dynamically differently (Smedsrud et al., 2013). The Barents Sea is a shallow 450-m-deep opening in which the flow is mostly depth-independent and toward the Arctic, while the Fram Strait is a 2,600-m-deep opening that exchanges water with the Arctic in a flow structure that varies with depth. Transects used to calculate the strait transports are indicated in Figure 1. For HadGEM3, the CAA transport was calculated southward of the location used in HiGEM1.1 in the Labrador Sea. This is to capture the transport through passages in the Western CAA, which are not resolved in the lower resolution HiGEM1.1 simulation.

The near-conservation of mass at annual time scales in the Arctic necessitates that an increase in inflow to the Arctic in one strait must coincide with a weaker inflow or stronger outflow in the other straits to compensate. The interconnectivity between the straits is determined by calculating and analyzing correlations between the volume transports through all five Arctic-Subarctic straits and openings in the two coupled climate models. The transports in each strait are defined positive toward the Arctic, which means that the straits that compensate each other are always negatively correlated. All correlations are calculated at 0 lag using Pearson's formula. For HiGEM1.1, the cross correlations between the strait transports were also calculated at lags up to 20 years, but the highest correlations were always at 0 lag. To investigate the frequencies at which the strait transports are coherent, the time series were low- and high-pass filtered with a cutoff at 6 years. This distinction is somewhat arbitrary but chosen so that the low-pass-filtered data will exclude high-frequency interannual variability but still have some degrees of freedom left in the 130-year time series of HiGEM1.1 (Note that the HadGEM3 simulation is too short for this analysis). The conclusions do not change when using a 5 or 7-year cutoff.

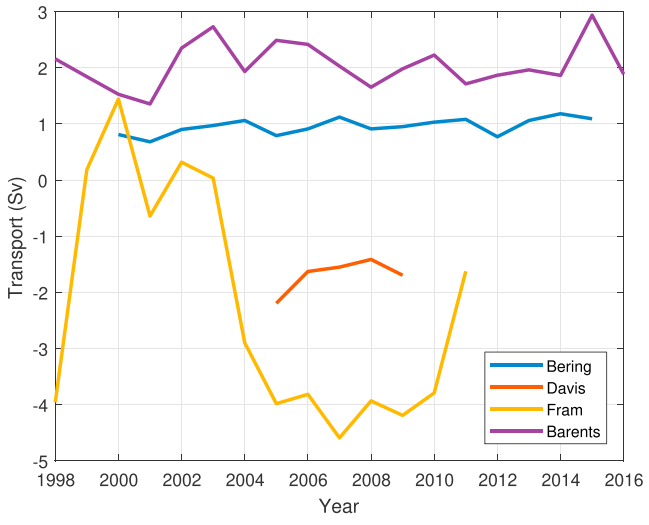

Figure 2. Observed annual mean volume transport in Sv through the Bering Strait (blue), Davis Strait (orange), Fram Strait (yellow), and Barents Sea Opening (purple). See text for sources.

In addition to correlations between the strait volume transports, we calculate correlations with five climate indices that were evaluated in the model, namely, (i) the North Atlantic Oscillation (NAO), defined as the mean sea level pressure (SLP) difference between Iceland and the Azores; (ii) the Arctic Oscillation (AO), defined as the first empirical orthogonal function of the SLP north of 20°N; (iii) the Aleutian Low Index (ALI), which is defined here as the longitude of the minimum of the SLP between 40 and 60°N and 150 and 210°E; (iv) the NINO3.4 index for the El Niño Southern Oscillation (ENSO), defined as the mean sea surface temperature anomaly in the equatorial East Pacific between 5°S and 5°N and 120 and 170°W; and (v) the maximum of the AMOC streamfunction at 40°N (AMOC40n).

3. Results: Coupled Climate Models

3.1. Comparison With Observations

We compare the mean of the annual volume transports time series across the Arctic Straits, indicated in Figure 1, and their associated annual standard deviations (*SD*) in the two climate models with the available observational data (Table 1 and Figure 2). The sources of the data are provided in

the data statement at the end of the paper. The transports refer to full depth-integrated ocean volume transports and are positive toward the Arctic (i.e., eastward for the Barents Sea and northward for all other sections). From the observations, we use only the years where transport data are available for the whole year. The imbalance of 0.2 Sv in the sum of the model strait flows arises from the precipitation-evaporation and the river runoff.

The mean transport through the Bering Strait from 2000 to 2015, as derived from the A3 mooring with correction for instrument depth and data dropout but without the correction for the Alaskan Coastal Current, is 1.0 ± 0.1 Sv (Woodgate, 2018; Woodgate et al., 2015). This agrees with the HiGEM1.1 Bering Strait transport of 1.2 ± 0.2 Sv and the HadGEM3 transport 1.1 ± 0.2 Sv. The CAA throughflow, estimated here by the observed mean transport through the Davis Strait for 2005–2009, is −1.7 ± 0.3 Sv (Curry et al., 2013). The HadGEM3 CAA transport of −2.0 ± 0.4 Sv is close to this estimate although the HiGEM1.1 transport of −0.8 ± 0.1 Sv is an underestimate in terms of both the mean transport and variability. The observed transport through the Barents Sea Opening between 1998 and 2016 is 2.1 ± 0.4 Sv (extension of Ingvaldsen et al., 2004). The Barents Sea HiGEM1.1 mean transport is 3.4 ± 0.5 Sv, and the HadGEM transport is 3.0 ± 0.4 Sv so that the observational estimate is about 1 Sv less than the model-derived transports, though with similar interannual variability. Finally, the measured mean transport through the Fram Strait between 1998 and 2011 is −2.2 ± 2.1 Sv (Beszczynska-Möller et al., 2015). This transport, from an array of 16 moorings between 7°W and 9°E, is highly variable. While the majority of the Fram Strait transport crosses this section, the exact contribution of the unresolved part on both the Svalbard shelf and the Greenland shelf is not really known from observations. Additionally, the central part of the deep Fram Strait where the recirculation displays a large eddy activity is ill-constrained by observations. Therefore, both the mean transport and the interannual variability are highly uncertain. Fram Strait is also the strait where the models disagree most, with transports of −4.0 ± 0.5 Sv in HiGEM1.1 and −2.3 ± 0.5 Sv in HadGEM3.

To summarize, the simulated Arctic straits transports are within the range of the observational estimates except that the mean volume transport and annual variability through the CAA in HiGEM1.1 are weaker than observed. There are only 5 years, 2005 to 2009, where annual transport estimates are available for all four straits. For these years the net mean annual transport into the Arctic through the four straits is −2.8 Sv. This imbalance implies that there is a considerable amount of transport not captured by available observations (Figure 2).

3.2. Interstrait Correlations

The cross correlations between the annual strait volume transports are shown in Table 2 for HiGEM1.1 (top) and HadGEM3 (bottom). The correlation coefficients of the straits transports with five climate indices will be discussed in section 4. There are three Arctic interstrait correlations that are significant (at 95% confidence level) and more than $|r| > 0.5$ in both models: (i) the Bering Strait and the Nordic Seas (HiGEM1.1: $r = -0.8$; HadGEM3: $r = -0.6$), (ii) the Nordic Seas and the CAA (HiGEM1.1: $r = -0.7$; HadGEM3: $r = -0.9$), and (iii) the Fram Strait and the Barents Sea (HiGEM1.1: $r = -0.9$; HadGEM3: $r = -0.5$). We name these three major interstrait connections respectively the Bering-Nordic connection (Figure 3, orange line), the Canadian-Nordic connection (Figure 3, blue line), and the Fram-Barents connection (Figure 3, red line). In HiGEM1.1 the Canadian-Nordic and the Fram-Barents correlations are a little stronger at periods longer than 6 years (i.e., low-pass-filtered) and the Bering-Nordic correlations are stronger at periods shorter than 6 years (i.e., high-pass-filtered; Table 3). Interestingly, there is no significant correlation between the Bering Strait and CAA transports in HadGEM3 or HiGEM1.1, either at short or long periods. Given that the Nordic Seas transport is the sum of the Fram Strait and Barents Sea transports, we investigate if the variability in the Nordic Seas is specifically related to one of these straits in particular. In HiGEM1.1, the Nordic Seas transport correlates best with the transport into the Barents Sea ($r = 0.4$), while in HadGEM3 it correlates best with the Fram Strait transport ($r = 0.7$).

Note that the correlations are different on a seasonal time scale. For instance, the monthly strait flows through the Nordic Seas and the CAA are positively correlated as both have strong outflows from the Arctic in the late summer, while on annual time scales they are negatively correlated. We focus here on the annual and longer timescale variability for which the Arctic throughflows are presumed to be in near balance.

Table 2
Correlations Between All Five Straits' Volume Transports and Five Climate Indices for HiGEM1.1 (top) and HadGEM3 (bottom)

HiGEM1.1	Bering	Nordic	CAA	Fram	Barents	NAO	AO	ALI	ENSO	AMOC
Bering	**1**	---	---	---	---	---	---	---	---	---
Nordic	**−0.8**	**1**	---	---	---	---	---	---	---	---
CAA		**−0.7**	**1**	---	---	---	---	---	---	---
Fram				**1**	---	---	---	---	---	---
Barents	**−0.3**	0.4	**−0.4**	**−0.9**	**1**	---	---	---	---	---
NAO	**−0.3**	0.4	**−0.3**		0.3	**1**	---	---	---	---
AO	**−0.5**	**0.6**	**−0.3**		0.3	**0.6**	**1**	---	---	---
ALI	**−0.5**	0.4					0.3	**1**	---	---
ENSO	0.3						**−0.4**		**1**	---
AMOC		0.4	**−0.5**							**1**
HadGEM3	Bering	Nordic	CAA	Fram	Barents	NAO	AO	ALI	ENSO	AMOC
Bering	**1**	---	---	---	---	---	---	---	---	---
Nordic	**−0.6**	**1**	---	---	---	---	---	---	---	---
CAA		**−0.9**	**1**	---	---	---	---	---	---	---
Fram	**−0.3**	**0.7**	**−0.7**	**1**	---	---	---	---	---	---
Barents				**−0.5**	**1**	---	---	---	---	---
NAO		**0.5**	**−0.5**			**1**	---	---	---	---
AO	**−0.6**	**0.6**	**−0.5**		0.3	**0.6**	**1**	---	---	---
ALI	**−0.5**							**1**	---	---
ENSO									**1**	---
AMOC	**−0.4**	0.4								**1**

Note. Correlations above 0.5 are in bold, and correlations below 95% confidence level or below 0.3 are not shown. The climate indices used here are as follows: NAO, North Atlantic Oscillation; AO, Arctic Oscillation; ALI, Aleutian Low Index describing the longitude of this low-pressure system; ENSO, El Niño Southern Oscillation; AMOC, maximum Atlantic Meridional Overturning Circulation streamfunction at 40°N.

4. Discussion: Mechanisms Behind Strait Correlations

There are two possible types of mechanisms for the strait correlations, causal and noncausal. An increase in the northward volume transport through an Arctic Strait would lead to sea level rise and an eventual adjustment in the volume transports of one or more of the other straits. This type of strait connectivity is causal (i.e., a perturbation in one strait leads directly to a perturbation in another). In reality the perturbation in any one

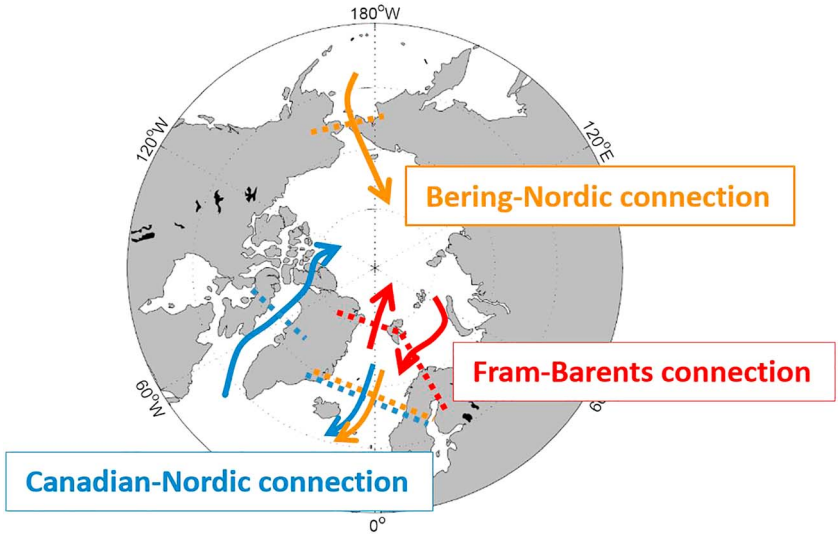

Figure 3. The three major strait connections identified through the inter-strait correlations; the Bering-Nordic connection (orange), the Canadian-Nordic connection (blue), and the Fram-Barents connection (red). The strait flows (and sections) that correlate strongly to each other are shown in the same color. Note that the arrows represent anomalous flow patterns and not the mean flow.

Table 3
Same as Table 2 But Here the Correlations Are Only for HiGEM1.1 and Are Calculated After the Time Series Were Low-Pass-Filtered (Top) and High-Pass-Filtered (Bottom) With the Cutoff at 6 Years

Low pass	Bering	Nordic	CAA	Fram	Barents	NAO	AO	ALI	ENSO	AMOC
Bering	**1.0**	---	---	---	---	---	---	---	---	---
Nordic	**−0.7**	**1.0**	---	---	---	---	---	---	---	---
CAA		**−0.8**	**1.0**	---	---	---	---	---	---	---
Fram				**1.0**	---	---	---	---	---	---
Barents		0.3	**−0.3**	**−0.9**	**1.0**	---	---	---	---	---
NAO		**0.6**	**−0.6**		0.3	**1.0**	---	---	---	---
AO	**−0.7**	**0.7**	**−0.3**		0.3	**0.5**	**1.0**	---	---	---
ALI	**−0.5**	0.4				0.3	0.4	**1.0**	---	---
ENSO	0.3			0.3	**−0.3**		**−0.5**		**1.0**	---
AMOC		0.4	**−0.6**			0.4				**1.0**
High pass	**Bering**	**Nordic**	**CAA**	**Fram**	**Barents**	**NAO**	**AO**	**ALI**	**ENSO**	**AMOC**
Bering	**1.0**	---	---	---	---	---	---	---	---	---
Nordic	**−0.9**	**1.0**	---	---	---	---	---	---	---	---
CAA		**−0.6**	**1.0**	---	---	---	---	---	---	---
Fram				**1.0**	---	---	---	---	---	---
Barents	**−0.4**	**0.5**	**−0.5**	**−0.8**	**1.0**	---	---	---	---	---
NAO	**−0.3**	0.3		**−0.3**	0.4	**1.0**	---	---	---	---
AO	**−0.5**	**0.6**	**−0.4**		0.4	**0.6**	**1.0**	---	---	---
ALI	**−0.5**	**0.5**					0.3	**1.0**	---	---
ENSO						**−0.3**	**−0.4**		**1.0**	---
AMOC	**−0.3**	0.3			0.3					**1.0**

strait is unlikely to be the sole response of a perturbation in another strait. A large-scale atmospheric pattern can drive opposite flows in two straits, resulting in a noncausal negative correlation between them (i.e., the common variability in both are forced externally and not from each other). In section 4.1, we first discuss the climate variables that are associated with anomalous transports in each strait and investigate potential common forcing mechanisms that could explain some of the major Arctic Strait connections we identified above. We then investigate causal mechanisms for strait correlations, that is, how strait flows adjust to each other directly.

4.1. Correlation Through Simultaneous External Forcing

4.1.1. The Bering-Nordic Connection

The northward transports through the Bering Strait and the Nordic Seas are significantly anticorrelated in both models, especially in HiGEM1.1 (Table 2). An anomalous SLP high in the central Arctic and low SLP in the North Pacific are associated with an anomalous northward volume transport in the Bering Strait and a southward transport in the Nordic Seas (Figures 4a and 4c). This atmospheric pattern is not local and stretches all the way to the subpolar North Atlantic where there is also a high SLP. As found by Danielson et al. (2014), the northward Bering Strait transport is associated with strong south-easterlies in the strait itself (Figure 4b). Southward of the strait, easterlies create a SSH high in the eastern Bering Sea, which enhances the meridional pressure gradient that drives a stronger northward flow through the strait (Danielson et al., 2014). North of the strait, easterly coastal winds set up a SSH low in the East Siberian Sea, as found by Peralta-Ferriz and Woodgate (2017), which further strengthen the meridional pressure gradient driven flow. Importantly for this study, a strong Bering Strait transport is also associated with northerly and north-westerly winds in the Nordic Seas and the Atlantic Subpolar gyre, which would be conducive to a southward transport through the Nordic Seas. Indeed, it is almost the exact opposite pattern obtained from regressing the winds onto the Nordic Seas transport (Figure 4d). Atmospheric and oceanic patterns in the Nordic Seas region are usually not considered when studying the dynamics of the Bering Strait flow (Danielson et al., 2014; Peralta-Ferriz & Woodgate, 2017).

The anomalous Nordic Seas flow and Bering Strait flows exhibit a qualitatively similar SLP, SSH, and wind stress pattern as that of the leading pattern of climate variability in the northern hemisphere, the AO (Figures 5c and 5d). Specifically, an anomalous SLP low in the central Arctic and SLP high in the subpolar North Pacific, together with a cyclonic wind stress pattern over the Subarctic, drive a northward flow anomaly from the Atlantic though the Nordic Seas and out through the Bering Strait into the Pacific. Indeed, the Nordic Seas

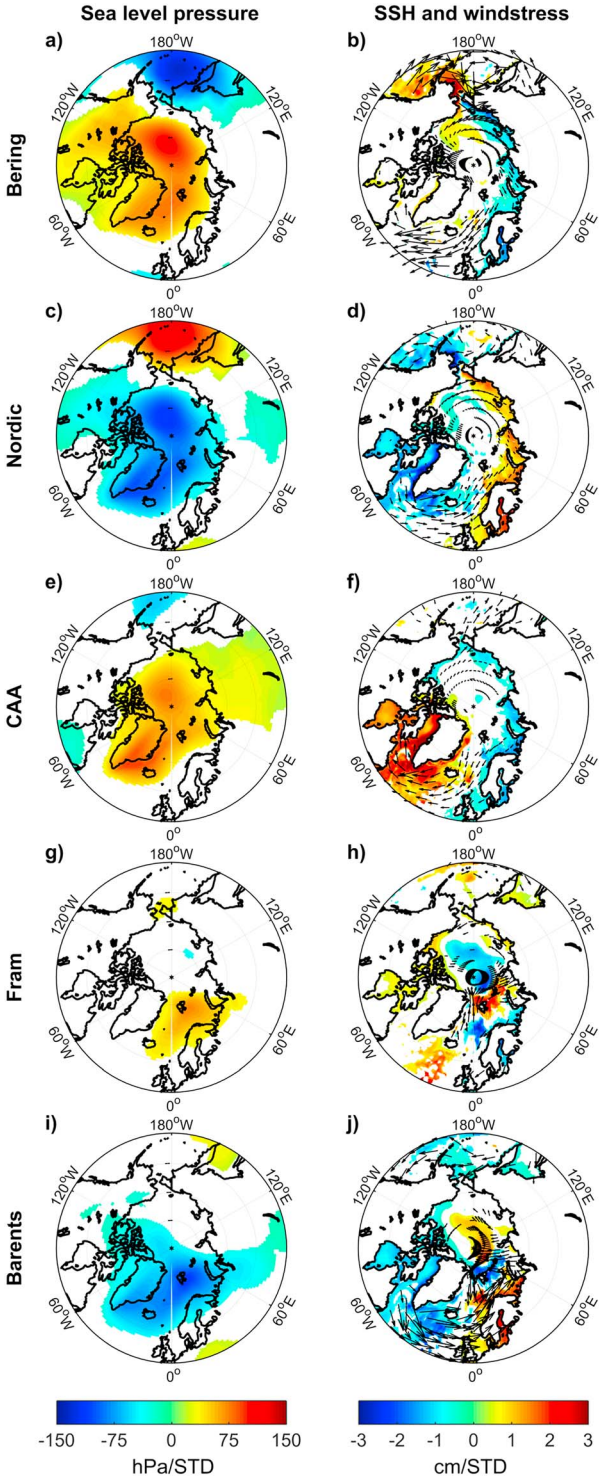

Figure 4. Regression coefficients of sea level pressure (first column) and sea surface height (SSH) and wind stress (second column) on the five strait transports associated with a 1 standard deviation increase in the respective strait volume transports. Only regression at 95% significance is displayed. The wind vectors are shown where either the regression of the meridional or zonal component is significant at 95%. The straits from top to bottom are the Bering Strait, the Nordic Seas opening, the Canadian Arctic Archipelago (CAA), the Fram Strait, and the Barents Sea opening.

transport and the AO are positively correlated (HiGEM and HadGEM: $r = 0.6$; Table 2) and the AO is negatively correlated with the Bering Strait transport (HiGEM: $r = -0.5$, HadGEM: $r = -0.6$; Table 2). The regression of SLP and SSH to the NAO shows similar features as the AO but not as pronounced (Figures 5a and 5b), and the correlation coefficients of the Nordic Seas and Bering Strait transports with the NAO are similar to that with the AO but typically 0.2 less (Table 2).

The strength of the Bering Strait transport has previously been connected to the longitudinal position of the Aleutian Low (Danielson et al., 2014). This ALI index (i.e., the longitudinal position of the Aleutian low) correlates significantly with the Bering Strait transport ($r = -0.5$ in both models) and to a lesser extent with the Nordic Seas transport in HiGEM ($r = 0.4$). When the Aleutian Low is shifted eastward, there is a low SLP anomaly over the central Arctic that is weaker but similar to the positive AO index (Figure 5e). This state is associated with anomalous northerly winds in the Bering Strait that weaken the mean northward flow and south-westerly winds in the Nordic Seas that contribute to the anomalous northward flow there (Figure 5f). As with the AO, this climate index does not appear to affect only the Bering Strait or the Nordic Seas but instead affects both simultaneously to some extent. To examine the importance of the strength (as opposed to longitudinal position) of the Aleutian Low, an additional index was calculated as the average SLP between 40 and 60°N and 160°E and 160°W. The correlation between this index and the Bering Strait transport was also significant ($r = -0.4$ in HiGEM) though somewhat weaker than with the index based on the longitude of the Aleutian Low and is not discussed further here. We find a weak correlation between the Bering Strait transport and ENSO ($r = 0.3$) in HiGEM. This may be related to a postulated connection between ENSO and the AO, with the Aleutian Low acting as a bridge between the two (Zhu & Wang, 2016). On the annual timescales here, the ENSO variability does not correlate significantly with SLP or SSH in the Atlantic sector of the Subarctic (Figures 5g and 5h) and is therefore unlikely responsible for noncausal correlations of the Bering-Nordic connection. Finally, the steric height difference between the Pacific and Atlantic has previously been invoked as a driver of the Pacific-Atlantic throughflow (Stigebrandt, 1984). Here in HiGEM1.1, the Bering Strait transport is not significantly correlated to the SSH in the central Arctic or Atlantic (Figure 4a) and only to a few small patches in the equatorial Pacific (not shown).

4.1.2. The Canadian-Nordic Connection

The CAA throughflow and the Nordic Seas throughflow are strongly anticorrelated ($r = -0.9$ in HadGEM3 model and $r = -0.7$ in HiGEM1.1). This connection has been noted before (Joyce & Proshutinsky, 2007; Lique et al., 2009). For instance, in the Drakkar eddy permitting model simulation of the 1965–2002 period, the correlation between the volume transports through the Fram Strait and Davis Strait was found to be $r = -0.84$ (Lique et al., 2009). Essentially, this anticorrelation describes an anomalous circulation around Greenland which, assuming a constant Bering Strait transport, can be calculated theoretically for a given wind field using Godfrey's Island rule (Godfrey, 1989; Joyce & Proshutinsky, 2007). However, in

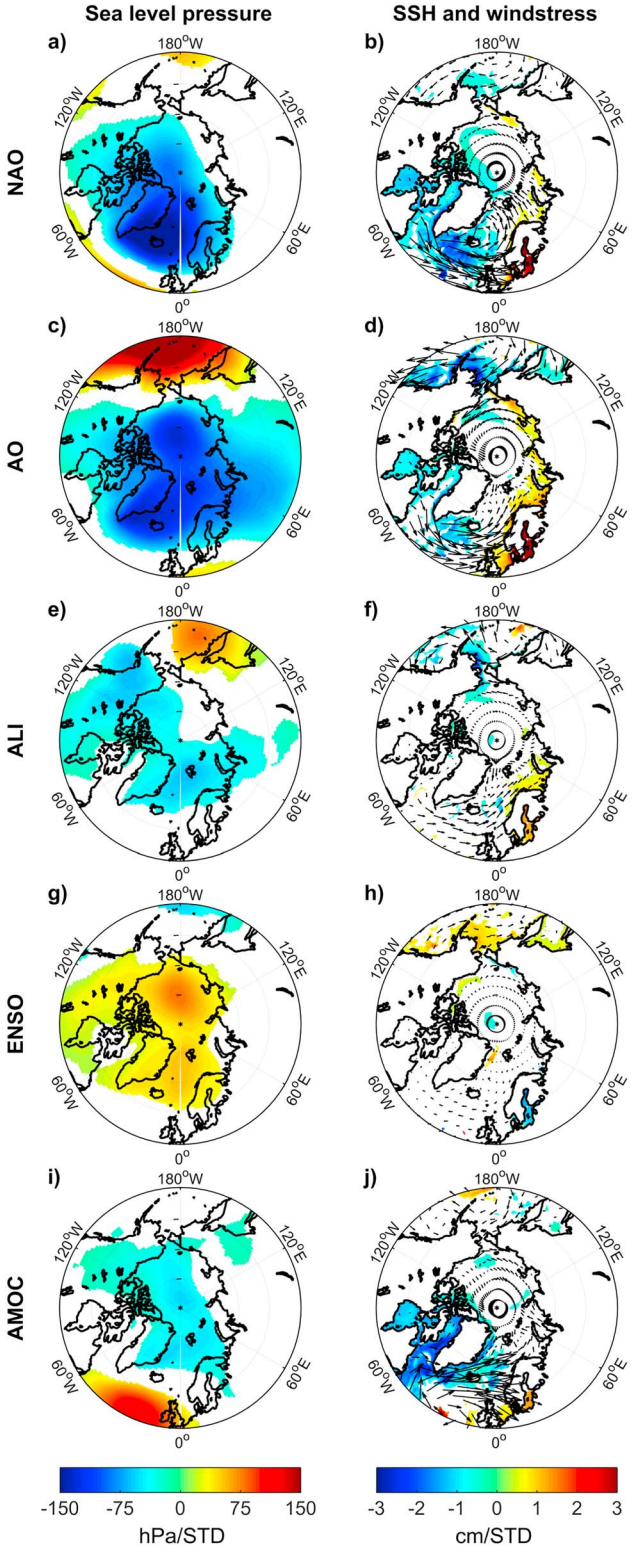

Figure 5. Same as in Figure 4 but sea level pressure (first column) and sea surface height (SSH) and wind stress (second column) are regressed on the five chosen climate indices. The climate indices are the same as in the text and Table 2, from top to bottom is the North Atlantic Oscillation (NAO), Arctic Oscillation (AO), Aleutian Low Index (ALI), El Niño Southern Oscillation (ENSO), and the Atlantic Meridional Overturning Circulation (AMOC).

reality the Bering Strait transport is not constant and its variability will affect either or both the CAA and Nordic Seas transports and potentially weakens the CAA-Nordic connection.

The common SLP pattern for anomalous northward CAA transport and southward Nordic seas transports is broadly similar to the negative AO SLP pattern, but this time the highest anomalous pressure is over the central Arctic and in particular eastern Greenland (Figures 4c and 4e). For such clockwise anomalous circulation around Greenland, the SLP over Greenland is higher and drives anomalous northerly and north-easterly winds in the Nordic Seas, and easterly winds south of Greenland (Figures 4d and 4f). Apart from anomalous south-easterly winds in the Labrador Sea region, there is no clear signal of anomalous winds over the CAA itself, which is consistent with several studies that found that the CAA volume transport is driven mostly by the upstream SSH, the downstream SSH, or the SSH gradient in the CAA (Houssais & Herbaut, 2011; Lu et al., 2014; McGeehan & Maslowski, 2012).

In HiGEM1.1, the CAA throughflow is highly correlated to the SSH in the whole CAA region (Figure 4f), especially along the western boundary. In other words, an anomalous northward CAA transport is linked to a higher SSH in the Canadian Archipelago. This type of SSH anomaly in the Canadian Archipelago is also a feature of a weaker than normal AMOC at 40°N (Figure 5j). The change in the ocean circulation associated with a weakening of the AMOC leads quasi-instantaneously to regional dynamic sea level rise (Levermann et al., 2005; Saenko et al., 2017). This has been observed in the North Atlantic; for example, a 128-mm jump in coastal sea level north of New York City in 2009–2010 has been associated with a 30% reduction of the AMOC (Goddard et al., 2015). In HiGEM1.1 the CAA transport is anticorrelated with the AMOC maximum streamfunction at 40°N ($r = -0.5$) and the correlation strengthens ($r = -0.6$) when both time series are low-pass filtered (cutoff period of 6 years; Table 3). This suggests that the CAA transport is coupled to AMOC variability on short period interannual timescales, and more so on longer timescales. The CAA-Nordic Seas correlation is somewhat stronger at the lower frequencies (Table 3).

4.1.3. The Fram-Barents Connection

The Nordic Sea transport reaches the Arctic through two openings, the Fram Strait and the Barents Sea, and the transports through these are anticorrelated in both HiGEM1.1 ($r = -0.9$) and HadGEM3 ($r = -0.5$). For an anomalous clockwise circulation around Svalbard (the island that splits these two openings to the Arctic), there is an anomalous local SLP high over Svalbard (Figure 4g, and opposite of Figure 4i). This SLP field leads to anticyclonic winds, which in turn create a local SSH high around Svalbard and adjacent SSH low centers north and south of this high (Figure 4h, opposite of Figure 4j). The resulting meridional SSH gradients drive the anticyclonic circulation around Svalbard. The opposite happens for a counterclockwise anomalous circulation around Svalbard. This mechanism has also been identified in observations on multiple timescales, from daily to interannual (Bader et al., 2011; Chafik et al., 2015; Lien et al., 2013; Lien et al., 2016). The counterclockwise phase of the Fram-Barents connection (i.e., anomalous Barents Sea transport towards the

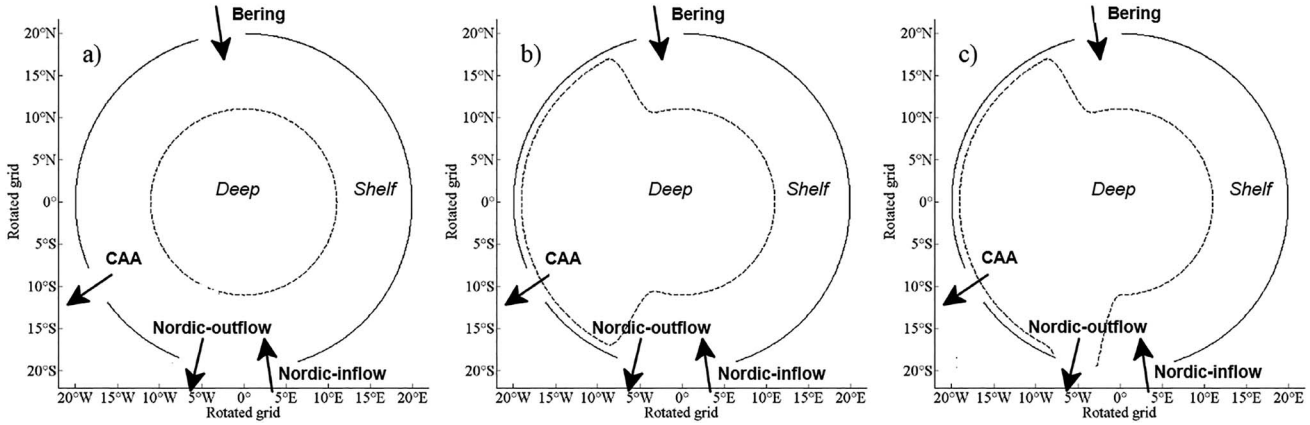

Figure 6. Bathymetry of the three idealized-basin simulations in NEMO3.6. The shelf is 250-m deep, and the total basin depth is 1,000 m. The four strait sections across which the volume transports are noted here as Bering (representing the Bering Strait), CAA (representing the Canadian Arctic Archipelago), the Nordic-outflow (representing the Fram Strait), and the Nordic-inflow (representing the Barents Sea).

Arctic) features a similar low SLP and cyclonic winds in the Nordic Seas as the AO and NAO. The Barents Sea transport is indeed weakly but significantly correlated to both in HiGEM1.1 ($r = 0.3$) as also found by Lien et al. (2016). In practice, the anomalous circulation around Svalbard can be facilitated by changing the fraction of the Atlantic Water carried by the Norwegian Atlantic Current that bifurcates into the Barents Sea versus the fraction that continues to feed the West Spitsbergen Current toward the Fram Strait. In summary, the Fram-Barents connection appears to be mostly a noncausal correlation in that there is an external atmospheric pattern that simultaneously drives both strait flows in opposite directions.

The discussion above focuses on the anticorrelation between the Fram Strait and the Barents Sea, but their sum makes up the Nordic Sea transport. It is of interest whether the Nordic Seas transport variability is facilitated mainly in the Barents Sea, or in the Fram Strait, or in both. In HiGEM1.1 the Nordic Seas transport is only significantly correlated with the Barents Sea transport ($r = 0.4$) and not with the Fram Strait. In HadGEM3, the Nordic Seas transport is only significantly correlated with the Fram Strait transport ($r = 0.7$) and the Fram Strait transport is also correlated with the Bering Strait (r = 0.3) and CAA ($r = -0.7$) transports. Considering that HadGEM3 provides a more detailed representation of the straits and mean transports closer to observations, the results tentatively suggest that Nordic Seas transport variability is mostly a response to or cause of Fram Strait transport variability. Given that these particular results are model dependent; this hypothesis would benefit from evaluation in future high-resolution coupled climate models.

4.2. Correlation Through Direct Adjustment

We investigate the causal nature of correlations through Arctic straits, in other words the direct adjustment of one strait transport to the anomaly in another. The focus here is on how a perturbation in the Bering Strait transport affects the SSH and circulation in the Arctic and the transport in the other straits. Toward this end, three simulations were set up in the NEMO ocean model (Figure 6) in which the bathymetric features become progressively more realistic: (i) a uniform-width step-shelf basin; (ii) an irregular-width step-shelf basin in which the western side of the shelf is narrower than the eastern side, thus more closely representing the real Arctic Ocean Continental Shelf; and (iii) a similar irregular-width step-shelf but with a deep channel in the western side of the Nordic Seas gap (i.e., a deep pseudo Fram Strait). In each case the shelf is 250-m deep, compared to the basin depth of 1,000 m.

The steady-state circulation is different for each of the three basin geometries (Figure 7, left column). In the first experiment with the basin with a uniform step-shelf width, the circulation is confined to the shelf, and in particular the western side (Figure 7a). The Nordic Seas inflow bifurcates into two branches: the first recirculates, exiting the western Nordic Sea opening, while the second branch flows toward the CAA to merge with the inflow from the Bering Strait and exit the domain. In the second experiment, in which the shelf is narrower on the western side, the Bering Strait inflow again circulates counterclockwise to exit in the CAA. Most of the transport is confined to the narrow shelf but a bottom friction controlled shelf edge boundary layer supports cross-shelf edge circulation that feeds a cyclonic deep basin current (Figure 7c). In the

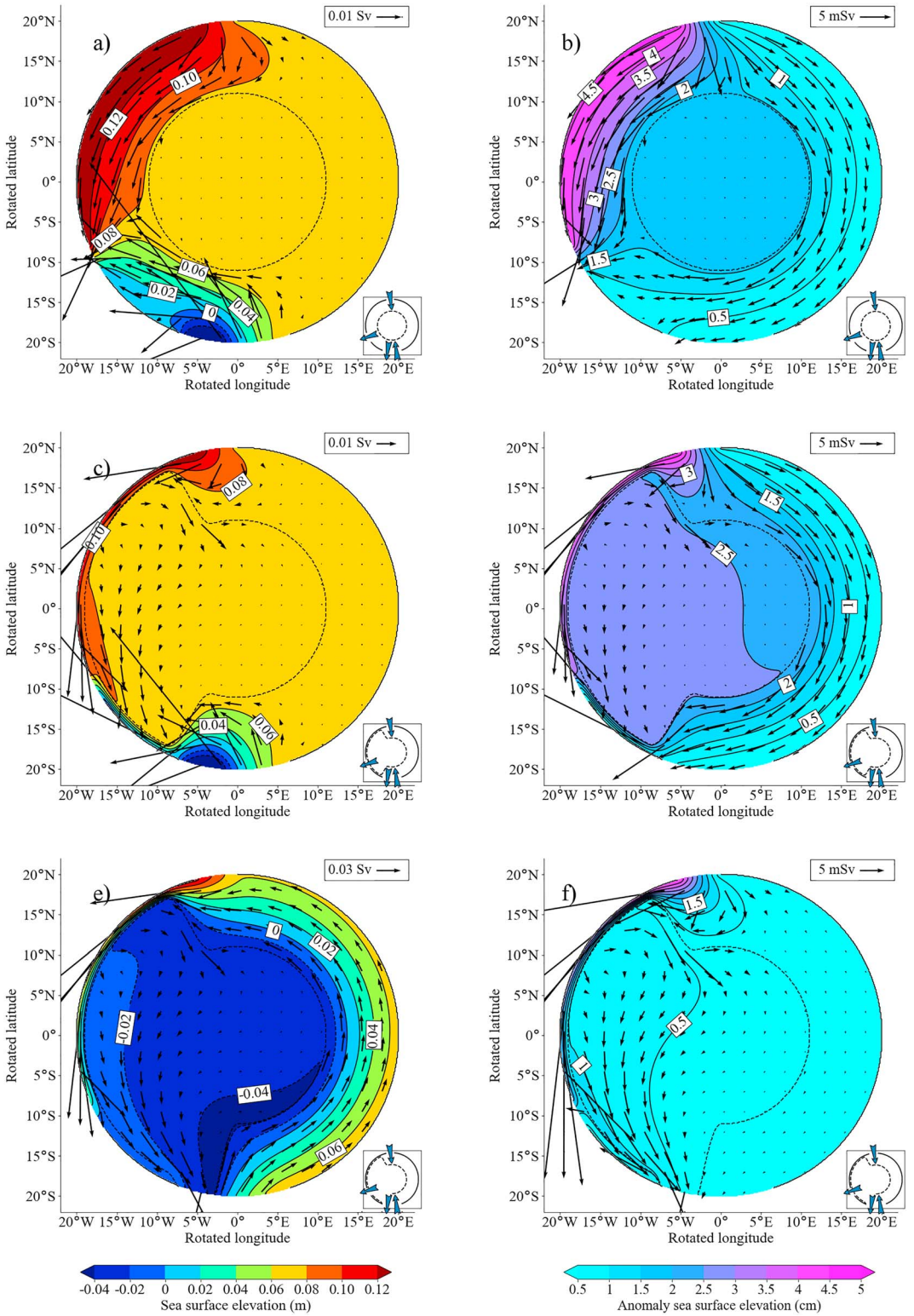

Figure 7. The steady-state depth-integrated transport vectors (in Sv) and the sea surface height anomaly contours for the control simulation of the three idealized-basin experiments (left column) and the anomalous transport vectors (in milli-Sverdrup, mSv) and sea surface height anomalies after the pseudo-Bering Strait perturbation (right column). The three rows correspond to the three basin geometries in Figure 6, and the corresponding basin bathymetries are shown here for reference in the inset at the bottom right of each subplot.

Table 4
Fraction (in %) of a 0.8 Sv Perturbation in the Bering Strait That is Adjusted in the Other Three Arctic Straits for the Three Different Basin Geometry Experiments in NEMO

	Uniform-width shelf	Irregular-width shelf	Irregular-width shelf with channel
CAA outflow	82	75	43
Nordic inflow branch	4	7	7
Nordic outflow branch	14	18	50

Nordic Seas, strong strait recirculation is again observed, with a fraction of the inflow exiting the domain through the CAA. In the third experiment with the deep channel in the western Nordic Seas gap, the circulation is quite different (Figure 7e). The inflowing Nordic strait transport flows cyclonically over the *wide eastern shelf* to merge with the Bering Strait inflow. Part of this merged current flows along the narrow shelf to exit at the CAA and the remaining current crosses the shelf break to form a deep basin circulation that exits through the deep Nordic channel.

In the perturbation experiments, the response of the circulation and strait flows to a 0.8-Sv increase in the Bering Strait inflow is studied (Figure 7, right column). For each of the three basin geometries, the percentage of the Bering Strait inflow increase that is adjusted in the CAA, the Nordic Seas inflow branch, and the Nordic Seas outflow branch is calculated (Table 4). In the first uniform-width shelf experiment, 82% of the perturbed Bering strait flow is accommodated through an increased outflow in the CAA and the remaining 18% in the Nordic Seas sections. In the second experiment with an irregular-width shelf, the adjustment in the CAA decreases to 75% and that in the Nordic Seas increases to 25%. In the third experiment with the deep channel in the western Nordic Seas section, the CAA now accommodates less than half of the adjustment at 43% with the remaining 57% exiting through the Nordic Seas section. The largest fraction of the Nordic Seas adjustment in each case is in the Nordic outflow branch, especially when this channel is deep (Table 4).

Taken at face value, the results suggest that the wider shelf in the eastern Arctic Ocean in conjunction with the deeper Fram Strait section leads to a preferential adjustment of a Bering Strait perturbation in the Fram Strait. That implies that the Bering-Nordic connection could at least in part be the result of local forcing in the Bering Strait leading to anomalies in the Bering Strait transport, which is then adjusted in the Nordic Seas. However, more work is needed to determine the sensitivity of the results to factors such as the control circulation, stratification, friction parameters, and basin geometry.

4.3. Complexities of Strait Connections

It is clear that some part of the interstrait volume transport connectivity is noncausal (i.e., due to simultaneous external forcing) and some part is causal (i.e., one strait adjusts to the anomaly in another strait). Yet it is nontrivial to extract or quantify the causal and noncausal contributions of the correlations for several reasons. The manner in which an anomalous transport in one strait is adjusted in the other straits can for instance be variable and depend on the mean flow and strength of transports in the other straits at that time. The correlations in strait volume transports can also not be directly attributed to correlations between major currents. In fact, the correlations break down when only upper layer transports are considered, for example, only transports above 1,000 m. Also, the variability in one strait, say the Nordic Seas, may be the response of variability in two other straits, one with a strong amplitude anomaly and one with a weak one. Even if the anomaly in the strait with the lower amplitude variability was fully adjusted in the Nordic Seas, it may be only weakly correlated to it, because the Nordic Seas variability will be dominated by the anomaly in the strait with the higher amplitude variability or by local forcing in the Nordic Seas.

A deeper understanding of the forcing of the strait flows may be attempted by determining at which frequencies the flows are coherent. For instance, the Bering-Nordic connection is stronger at shorter periods and the Canadian-Nordic connection at longer. Note though that coherence of the transports through two straits at decadal periods can mean that both are forced by an external forcing at this period or that only one strait is forced at this period and the other adjusts within days to months. The same could be said for strait transports that are coherent at shorter interannual periods. The frequency analysis therefore does not on its own distinguish between causal and noncausal correlations.

5. Summary and Conclusions

This work investigates the interconnectivity of the volume transports through the Arctic straits and the causal or noncausal nature of their relationship, that is, whether they are simultaneously forced or whether the one is responding to the other. The strait volume transport correlations are investigated in two global climate models: the HiGEM1.1 model, which has a 1/3° horizontal resolution in the ocean and a 130-year control simulation, and the HadGEM3 model, which has a nominal 1/12° horizontal ocean resolution and a 39-year control simulation. The focus is on annual mean data given that the oceanic volume transports do not balance on monthly timescales as water is locked up in sea ice over winter and released in summer months.

We identified three pairs of straits whose transports covary strongly with each other (in opposite directions) in both models, the Bering Strait and the Nordic Seas, the Nordic Seas and the CAA, and the Fram Strait and the Barents Sea. These strait connections suggest the following three main anomalous flow patterns through the Arctic: (1) the Bering-Nordic connection, in which there is a transport from the Pacific to the Atlantic through the Bering Strait and Nordic Seas; (2) the Canadian-Nordic connection, which relates to an anomalous circulation around Greenland; and (3) the Fram-Barents connection, which describes an anomalous circulation around Svalbard. It is too early to say whether Nordic Sea transport variability is mostly connected to variability in the Fram Strait or the Barents Sea because of model discrepancies. In HiGEM1.1 the Nordic Seas transport correlates more strongly with the Barents Sea transport, and in HadGEM3 the Nordic Seas transport correlates more strongly with the Fram Strait transport.

All three interstrait connections are to some extent noncausal in that they are the result of both straits in question being affected by the same large scale atmospheric SLP patterns. For instance, for the Bering-Nordic connection, there is an anomalous SLP low over the central Arctic, similar to the SLP pattern of the AO. North-westerly winds in the Bering Strait and southerly winds in the Nordic Seas induce an anomalous southward transport in the Bering Strait and northward transport in the Nordic Seas, respectively. For the Canadian-Nordic connection there is a similar SLP pattern, but here it is more focused on Eastern Greenland. A SLP low there drives cyclonic winds around Greenland that help drive an anomalous northward flow in the Nordic Seas. It may also contribute to the SSH low in the CAA, which helps to drive the anomalous CAA transport from the Arctic. The SSH low in the CAA could also be related to the AMOC. A similar SSH low in the CAA is found for a strong AMOC, and the AMOC index at 40°N is anticorrelated to the CAA volume transport. Finally, the atmospheric signal of the Fram-Barents connection is a strong local SLP anomaly over Svalbard with two opposing SLP centers to the north and south. When the SLP anomaly is negative, there are cyclonic winds around Svalbard simultaneously driving a north-eastward flow anomaly in the Barents Sea and a southward flow anomaly in the Fram Strait.

The correlations described above are significant but explain only part of the variance of the strait transport anomalies. The straits flows are also affected by other atmospheric patterns such as the Aleutian Low and more random variability. Importantly, the atmospheric forcing regime during any given year, whether associated with a familiar climate mode or not, is unlikely to fortuitously cause the strait transports to exactly balance each other. The imbalance will create sea level anomalies. Subsequent waves restore the overall balance. That begs the questions of how and where the balance is restored. The NEMO barotropic circular basin experiments in this study allow insight into the controls on the causal relationship between straits. In other words, if there is a transport perturbation in one strait, how and where will it be compensated to ensure mass balance. Here we focused on the adjustment to perturbations in the Bering Strait. The coupled climate model simulation suggested that the Bering Strait variability is compensated in the Nordic Seas and not the CAA. Three simple basin geometries were tested to establish the essential bathymetric features necessary to capture this relationship. For a circular even-width shelf around the Arctic, the Bering Strait anomaly was mostly compensated in the CAA (82%). The introduction of a narrower shelf on the western side than the eastern side slightly reduced the fraction of the Bering Strait anomaly that exited in the CAA (75%) and increased that which exited through Nordic Seas section to 25%. Yet only when a deep channel was introduced in the western part of the Nordic Section was the Bering Strait anomaly mostly adjusted through the Nordic Seas (57%).

Despite the complexities of the strait connections, and the fact that long transport records covering all straits are currently lacking, there are ways forward to better understand the straits connectivity and distinguish between local forcing and strait-adjustment. Determining the strait connections in a set of models that

have reasonable Arctic Strait representation and long simulations would be most valuable; this would allow independent assessment of the robustness of the interstrait connectivity reported here. Furthermore, we suggest that a useful direction of study would be to develop idealized experiments to identify how altered high-latitude bathymetry, winds, and background circulation state may affect Arctic strait transport connectivity. Finally, targeted forcing (e.g., anomalous local winds) of different strait transports in realistic ocean models will also help to better understand strait dynamics.

Acknowledgments

HiGEM1.1 was developed from the Met Office Hadley Centre Model by the UK High-Resolution Modelling Project and the UK Japan Climate Collaboration (UJCC) and was supported by NERC, the Foreign and Commonwealth Office Global Opportunities Fund, and the DECC/Defra Met Office Hadley Centre Climate Programme. The model integrations were performed using the Japanese Earth Simulator supercomputer, supported by JAMSTEC. The work of Pier Luigi Vidale and Malcolm Roberts in leading the effort in Japan is particularly valued. HadGEM3 was developed by the UK Met Office, and the high-resolution integration was undertaken by Andrew Coward as part of the NERC ACSIS program (NE/N018044/1). This work used the ARCHER UK National Supercomputing Service. Model analysis was carried out on resources provided by the Swedish National Infrastructure for Computing (SNIC) at the National Supercomputer Centre (NSC). De Boer gratefully acknowledges support from the Swedish Research Council project (2016-03912). Zhang was supported through the Swedish Research Council for the Swedish-French project GIWA. Stevens gratefully acknowledges funding from NERC [NE/M006069/1]. Chafik acknowledges support from the Swedish National Space Board (SNSB; Dnr 133/17). All modeling output used to produce the figures in this paper are available at https://bolin.su.se/data/DeBoer-2018. We gratefully acknowledge provision of the transport measurements. The data can be obtained as follows. The Bering Strait data are stored at http://psc.apl.washington.edu/HLD/Bstrait/bstrait.html, the Fram Strait transports are at https://doi.org/10.1594/PANGAEA.150016, the Davis Strait data are available from Beth Curry (beth4-cu@uw.edu), and the Barents Sea Opening transports are available from Randi Ingvaldsen (randi.ingvaldsen@hi.no).

References

Armitage, T. W. K., Bacon, S., Ridout, A. L., Thomas, S. F., Aksenov, Y., & Wingham, D. J. (2016). Arctic Sea surface height variability and change from satellite radar altimetry and GRACE, 2003–2014. *Journal of Geophysical Research: Oceans*, *121*, 4303–4322. https://doi.org/10.1002/2015JC011579

Bader, J., Mesquita, M. D. S., Hodges, K. I., Keenlyside, N., Østerhus, S., & Miles, M. (2011). A review on Northern Hemisphere sea-ice, storminess and the North Atlantic Oscillation: Observations and projected changes. *Atmospheric Research*, *101*(4), 809–834. http://www.sciencedirect.com/science/article/pii/S0169809511001001. https://doi.org/10.1016/j.atmosres.2011.04.007

Beszczynska-Möller, A., von Appen, W.-J., & Fahrbach, E. (2015). Physical oceanography and current meter data from moorings F1-F14 and F15/F16 in the Fram Strait, 1997–2012. Retrieved from: https://doi.org/10.1594/PANGAEA.150016

Beszczynska-Möller, A., Woodgate, R. A., Lee, L., Melling, H., & Karcher, M. (2011). A synthesis of exchanges through the main oceanic gateways to the Arctic Ocean. *Oceanography*, *24*(3), 83–99.

Bhatt, U. S., Walker, D. A., Walsh, J. E., Carmack, E. C., Frey, K. E., Meier, W. N., et al. (2014). Implications of Arctic sea ice decline for the Earth System. *Annual Review of Environment and Resources*, *39*(1), 57–89. https://doi.org/10.1146/annurev-environ-122012-094357

Chafik, L., Nilsson, J., Skagseth, Ø., & Lundberg, P. (2015). On the flow of Atlantic water and temperature anomalies in the Nordic Seas toward the Arctic Ocean. *Journal of Geophysical Research: Oceans*, *120*, 7897–7918. https://doi.org/10.1002/2015JC011012

Conkright M.E., Locarnini, R. A., Garcia, H. E., O'Brien, T., Boyer, T. P., Stephens, C., & Antonov, J. I. (2002). World Ocean Atlas 2001: Objective analyses, data statistics, and figures CD-ROM documentation. NODC Internal Report 17, 17 pp.

Curry, B., Lee, C. M., Petrie, B., Moritz, R. E., & Kwok, R. (2013). Multiyear volume, liquid freshwater, and sea ice transports through Davis Strait, 2004–10. *Journal of Physical Oceanography*, *44*(4), 1244–1266. https://doi.org/10.1175/JPO-D-13-0177.1

Danielson, S. L., Weingartner, T. J., Hedstrom, K. S., Aagaard, K., Woodgate, R., Curchitser, E., & Stabeno, P. J. (2014). Coupled wind-forced controls of the Bering–Chukchi shelf circulation and the Bering Strait throughflow: Ekman transport, continental shelf waves, and variations of the Pacific–Arctic sea surface height gradient. *Progress in Oceanography*, *125*, 40–61. https://doi.org/10.1016/j.pocean.2014.04.006

De Boer, A. M., Graham, R. M., Thomas, M. D., & Kohfeld, K. E. (2013). The control of the southern hemisphere westerlies on the position of the subtropical front. *Journal of Geophysical Research: Oceans*, *118*, 5669–5675. https://doi.org/10.1002/jgrc.20407

De Boer, A. M., & Nof, D. (2004a). The Bering Strait is grip on the northern hemisphere climate. *Deep-sea Research Part I-oceanographic Research Papers*, *51*(10), 1347–1366.

De Boer, A. M., & Nof, D. (2004b). The exhaust valve of the North Atlantic. *Journal of Climate*, *17*(3), 417–422.

Dickson, R. R., Osborn, T. J., Hurrell, J. W., Meincke, J., Blindheim, J., Adlandsvik, B., et al. (2000). The Arctic Ocean response to the North Atlantic Oscillation. *Journal of Climate*, *13*(15), 2671–2696. https://doi.org/10.1175/1520-0442(2000)013<2671:TAORTT>2.0.CO;2

Flather, R. A. (1994). A storm surge prediction model for the Northern Bay of Bengal with application to the cyclone disaster in April 1991. *Journal of Physical Oceanography*, *24*(1), 172–190. http://journals.ametsoc.org/doi/abs/10.1175/1520-0485(1994)024%3C0172%3AASSPMF%3E2.0.CO%3B2

Gent, P. R., & McWilliams, J. C. (1990). Isopycnal mixing in ocean circulation models. *Journal of Physical Oceanography*, *20*(1), 150–155. <Go to ISI>://A1990CM51600012

Goddard, P. B., Yin, J., Griffies, S. M., & Zhang, S. (2015). An extreme event of sea-level rise along the northeast coast of North America in 2009–2010. *Nature Communications*, *6*(1), 6346. https://doi.org/10.1038/ncomms7346

Godfrey, J. S. (1989). A sverdrup model of the depth-integrated flow for the world ocean allowing for island circulations. *Geophysical and Astrophysical Fluid Dynamics*, *45*(1–2), 89–112. https://doi.org/10.1080/03091928908208894

Graham, R. M., De Boer, A. M., Heywood, K. J., Chapman, M. R., & Stevens, D. P. (2012). Southern Ocean fronts: Controlled by wind or topography. *Journal of Geophysical Research*, *117*, C08018. https://doi.org/10.1029/2012JC007887

Griffies, S. M. (1998). The Gent-McWilliams skew flux. *Journal of Physical Oceanography*, *28*(5), 831–841. <Go to ISI>://000073762900006

Houssais, M.-N., & Herbaut, C. (2011). Atmospheric forcing on the Canadian Arctic Archipelago freshwater outflow and implications for the Labrador Sea variability. *Journal of Geophysical Research*, *116*, C00D02. https://doi.org/10.1029/2010JC006323

Hu, A. X., & Meehl, G. A. (2005). Bering Strait throughflow and the thermohaline circulation. *Geophysical Research Letters*, *32*, L24610. https://doi.org/10.1029/2005GL024424

Hu, A. X., Meehl, G. A., Otto-Bliesner, B. L., Waelbroeck, C., Han, W. Q., Loutre, M. F., et al. (2010). Influence of Bering Strait flow and North Atlantic circulation on glacial sea-level changes. *Nature Geoscience*, *3*(2), 118–121. https://doi.org/10.1038/ngeo729

Ingvaldsen, R. B., Asplin, L., & Loeng, H. (2004). Velocity field of the western entrance to the Barents Sea. *Journal of Geophysical Research*, *109*, C03021. https://doi.org/10.1029/2003JC001811

Intergovernmental Panel on Climate Change (2013). *Climate change 2007—The physical science basis: Working group I contribution to the 5th assessment report of the IPCC* (Vol. 4). Cambridge, UK: Cambridge University Press.

Johnson, H. L., Cornish, S. B., Kostov, Y., Beer, E., & Lique, C. (2018). Arctic Ocean freshwater content and its decadal memory of sea-level pressure. *Geophysical Research Letters*, *45*, 4991–5001. https://doi.org/10.1029/2017GL076870

Joyce, T. M., & Proshutinsky, A. (2007). Greenland's island rule and the Arctic Ocean circulation. *Journal of Marine Research*, *65*(5), 639–653. http://www.ingentaconnect.com/content/jmr/jmr/2007/00000065/00000005/art00003. https://doi.org/10.1357/002224007783649439

Koenigk, T., Mikolajewicz, U., Haak, H., & Jungclaus, J. (2007). Arctic freshwater export in the 20th and 21st centuries. *Journal of Geophysical Research*, *112*, G04S41. https://doi.org/10.1029/2006JG000274

Levermann, A., Griesel, A., Hofmann, M., Montoya, M., & Rahmstorf, S. (2005). Dynamic sea level changes following changes in the thermohaline circulation. *Climate Dynamics*, *24*(4), 347–354. <Go to ISI>://000227945800002

Lien, V. S., Schlichtholz, P., Skagseth, Ø., & Vikebø, F. B. (2016). Wind-driven Atlantic water flow as a direct mode for reduced Barents Sea ice cover. *Journal of Climate*, *30*(2), 803–812. https://doi.org/10.1175/JCLI-D-16-0025.1

Lien, V. S., Vikebø, F. B., & Skagseth, Ø. (2013). One mechanism contributing to co-variability of the Atlantic inflow branches to the Arctic. *Nature Communications*, *4*, 1488. https://doi.org/10.1038/ncomms2505

Lique, C., & Johnson, H. L. (2015). Is there any imprint of the wind variability on the Atlantic water circulation within the Arctic Basin? *Geophysical Research Letters*, *42*, 9880–9888. https://doi.org/10.1002/2015GL066141

Lique, C., Treguier, A. M., Scheinert, M., & Penduff, T. (2009). A model-based study of ice and freshwater transport variability along both sides of Greenland. *Climate Dynamics*, *33*(5), 685–705. https://doi.org/10.1007/s00382-008-0510-7

Lu, Y., Higginson, S., Nudds, S., Prinsenberg, S., & Garric, G. (2014). Model simulated volume fluxes through the Canadian Arctic Archipelago and Davis Strait: Linking monthly variations to forcing in different seasons. *Journal of Geophysical Research: Oceans*, *119*, 1927–1942. https://doi.org/10.1002/2013JC009408

Luneva, M. V., Willmott, A. J., & Maqueda, M. A. M. (2012). Geostrophic adjustment problems in a polar basin. *Atmosphere-Ocean*, *50*(2), 134–155. https://doi.org/10.1080/07055900.2012.659719

Madec, G. (2016). NEMO ocean engine. *Note du Pole de modelisation de l'Institut Pierre-Simon Laplace (IPSL)*, Technical Report 27.

Mauritzen, C., & Häkkinen, S. (1997). Influence of sea ice on the thermohaline circulation in the Arctic-North Atlantic Ocean. *Geophysical Research Letters*, *24*(24), 3257–3260. https://doi.org/10.1029/97GL03192

McGeehan, T., & Maslowski, W. (2012). Evaluation and control mechanisms of volume and freshwater export through the Canadian Arctic Archipelago in a high-resolution pan-Arctic ice-ocean model. *Journal of Geophysical Research*, *117*, C00D14. https://doi.org/10.1029/2011JC007261

Otterå, O. H., Drange, H., Bentsen, M., Kvamstø, N. G., & Jiang, D. (2003). The sensitivity of the present-day Atlantic Meridional Overturning Circulation to freshwater forcing. *Geophysical Research Letters*, *30*(17), 1898. https://doi.org/10.1029/2003GL017578

Peralta-Ferriz, C., & Woodgate, R. A. (2017). The dominant role of the east Siberian Sea in driving the oceanic flow through the Bering Strait—Conclusions from GRACE Ocean mass satellite data and in situ mooring observations between 2002 and 2016. *Geophysical Research Letters*, *44*, 11,472–411,481. https://doi.org/10.1002/2017GL075179

Roberts, M. J., Clayton, A., Demory, M. E., Donners, J., Vidale, P. L., Norton, W., et al. (2009). Impact of resolution on the tropical Pacific circulation in a matrix of coupled models. *Journal of Climate*, *22*(10), 2541–2556. https://doi.org/10.1175/2008JCLI2537.1

Roberts, M. J., & Marshall, D. (1998). Do we require adiabatic dissipation schemes in eddy-resolving ocean models? *Journal of Physical Oceanography*, *28*(10), 2050–2063. <Go to ISI>://000076634200011

Saenko, O. A., Yang, D., & Myers, P. G. (2017). Response of the North Atlantic dynamic sea level and circulation to Greenland meltwater and climate change in an eddy-permitting ocean model. *Climate Dynamics*, *49*(7-8), 2895–2910. https://doi.org/10.1007/s00382-016-3495-7

Sevellec, F., Fedorov, A. V., & Liu, W. (2017). Arctic sea-ice decline weakens the Atlantic Meridional Overturning Circulation. *Nature Climate Change*, *7*(8), 604–610. https://doi.org/10.1038/nclimate3353

Shaffrey, L. C., Stevens, I., Norton, W. A., Roberts, M. J., Vidale, P. L., Harle, J. D., et al. (2009). U.K. HiGEM: The new U.K. high-resolution global environment model—Model description and basic evaluation. *Journal of Climate*, *22*(8), 1861–1896. https://doi.org/10.1175/2008JCLI2508.1

Smedsrud, L. H., Esau, I., Ingvaldsen, R. B., Eldevik, T., Haugan, P. M., Li, C., et al. (2013). The role of the Barents Sea in the Arctic climate system. *Reviews of Geophysics*, *51*, 415–449. https://doi.org/10.1002/rog.20017

Stigebrandt, A. (1984). The North Pacific: A global-scale estuary. *Journal of Physical Oceanography*, *14*(2), 464–470. https://doi.org/10.1175/1520-0485(1984)014<0464:TNPAGS>2.0.CO;2

Storkey, D., Blaker, A. T., Mathiot, P., Megann, A., Aksenov, Y., Blockley, E. W., et al. (2018). UK Global Ocean GO6 and GO7: A traceable hierarchy of model resolutions. *Geoscientific Model Development Discussion*, *2018*, 1–43. https://www.geosci-model-dev-discuss.net/gmd-2017-263/

Stroeve, J., Holland, M. M., Meier, W., Scambos, T., & Serreze, M. (2007). Arctic Sea ice decline: Faster than forecast. *Geophysical Research Letters*, *34*, L09501. https://doi.org/10.1029/2007GL029703

Sutton, R. T., McCarthy, G. D., Robson, J., Sinha, B., Archibald, A. T., & Gray, L. J. (2017). Atlantic multidecadal variability and the U.K. ACSIS program. *Bulletin of the American Meteorological Society*, *99*(2), 415–425. https://doi.org/10.1175/BAMS-D-16-0266.1

Thomas, M. D. (2012). *Sverdrup balance and three dimensional variability of the Meridional Overturning Circulation*. (Ph.D.), University of East Anglia, Norwich.

Williams, K. D., Copsey, D., Blockley, E. W., Bodas-Salcedo, A., Calvert, D., Comer, R., et al. (2017). The Met Office Global Coupled Model 3.0 and 3.1 (GC3.0 and GC3.1) Configurations. *Journal of Advances in Modeling Earth Systems*, *10*, 357–380. https://doi.org/10.1002/2017MS001115

Woodgate, R. A. (2018). Increases in the Pacific inflow to the Arctic from 1990 to 2015, and insights into seasonal trends and driving mechanisms from year-round Bering Strait mooring data. *Progress in Oceanography*, *160*, 124–154. https://doi.org/10.1016/j.pocean.2017.12.007

Woodgate, R. A., Aagaard, K., & Weingartner, T. J. (2006). Interannual changes in the Bering Strait fluxes of volume, heat and freshwater between 1991 and 2004. *Geophysical Research Letters*, *33*, L15609. https://doi.org/10.1029/2006GL026931

Woodgate, R. A., Stafford, K. M., & Prahl, F. G. (2015). A synthesis of year-round interdisciplinary mooring measurements in the Bering Strait (1990–2014) and the RUSALCA years (2004–2011). *Oceanography*, *28*, 46–67. https://doi.org/10.5670/oceanog.2015.57

Yang, Q., Dixon, T. H., Myers, P. G., Bonin, J., Chambers, D., van den Broeke, M. R., et al. (2016). Recent increases in Arctic freshwater flux affects Labrador Sea convection and Atlantic overturning circulation. *Nature Communications*, *7*, 10525. https://doi.org/10.1038/ncomms10525

Zhu, Y., & Wang, T. (2016). The relationship between the Arctic Oscillation and ENSO as simulated by CCSM4. *Atmospheric and Oceanic Science Letters*, *9*(3), 198–203. https://doi.org/10.1080/16742834.2016.1149287